Nephron

Experimental Nephrology and Genetics: Research Article

Nephron 2024;148:487–502
DOI: 10.1159/000535918

Received: June 7, 2023
Accepted: December 4, 2023
Published online: February 14, 2024

Shared and Distinct Renal Transcriptome Signatures in 3 Standard Mouse Models of Chronic Kidney Disease

Adam B. Marstrand-Jørgensen[a] Frederikke Emilie Sembach[a] Stine Thorhauge Bak[a] Maria Ougaard[a] Mikkel Christensen-Dalsgaard[a] Martin Rønn Madsen[a] Ditte Marie Jensen[a] Thomas Secher[a, b] Sebastian Møller Nguyen Heimbürger[a] Lisbeth N. Fink[a, c] Ditte Hansen[d, e] Henrik H. Hansen[a] Mette Viberg Østergaard[a, f] Michael Christensen[a] Louise S. Dalbøge[a]

[a]Gubra A/S, Hørsholm, Denmark; [b]Cell Imaging and Pharmacology, Cell Therapy R&D, Novo Nordisk A/S, Måløv, Denmark; [c]Biotherapeutics Screening, Ferring Pharmaceuticals A/S, Kastrup, Denmark; [d]Department of Nephrology, Herlev-Gentofte Hospital, University of Copenhagen, Herlev, Denmark; [e]Department of Clinical Medicine, University of Copenhagen, Copenhagen, Denmark; [f]Novo Nordisk A/S, Måløv, Denmark

Keywords
Chronic kidney disease · Mouse models · Transcriptomics · Unilateral ureter obstruction · Unilateral ischemia-reperfusion injury · Adenine-induced nephropathy

Abstract

Introduction: Several mouse models with diverse disease etiologies are used in preclinical research for chronic kidney disease (CKD). Here, we performed a head-to-head comparison of renal transcriptome signatures in standard mouse models of CKD to assess shared and distinct molecular changes in three mouse models commonly employed in preclinical CKD research and drug discovery. ***Methods:*** All experiments were conducted on male C57BL/6J mice. Mice underwent sham, unilateral ureter obstruction (UUO), or unilateral ischemic-reperfusion injury (uIRI) surgery and were terminated two- and 6-weeks post-surgery, respectively. The adenine-supplemented diet-induced (ADI) model of CKD was established by feeding with adenine diet for 6 weeks and compared to control diet feeding. For all models, endpoints included plasma biochemistry, kidney histology, and RNA sequencing. ***Results:*** All models displayed increased macrophage infiltration (F4/80 IHC) and fibrosis (collagen 1a1 IHC). Compared to corresponding controls, all models were characterized by an extensive number of renal differentially expressed genes (≥11,000), with a notable overlap in transcriptomic signatures across models. Gene expression markers of fibrosis, inflammation, and kidney injury supported histological findings. Interestingly, model-specific transcriptome signatures included several genes representing current drug targets for CKD, emphasizing advantages and limitations of the three CKD models in preclinical target and drug discovery. ***Conclusion:*** The UUO, uIRI, and ADI mouse models of CKD have significant commonalities in their renal global transcriptome

karger@karger.com
www.karger.com/nef

Correspondence to:
Louise S. Dalbøge, lsd@gubra.dk

Karger

profile. Model-specific renal transcriptional signatures should be considered when selecting the specific model in preclinical target and drug discovery.

Introduction

Chronic kidney disease (CKD) is characterized by progressive kidney damage and loss of function in the kidneys, determined by decreased glomerular filtration rate (GFR) and albuminuria [1]. Development of fibrosis is a common driver of CKD and a hallmark of disease progression, which may ultimately result in kidney failure [2]. Given the significant effect of CKD on cardiovascular risk and end-stage kidney disease, CKD represents a growing disease burden and is among the fastest growing causes of mortality worldwide. Accordingly, CKD is considered implicated in more than 2% of all deaths and affects more than 10% of the global population [3, 4]. The etiology of CKD varies, with many types of CKD caused by glomerular and tubulointerstitial disease or injury [5]. More than half of all cases of CKD are complications of common cardiometabolic conditions such as diabetes and hypertension [6].

The development of new and more effective CKD-targeting drugs has proven to be challenging. As a result, lifestyle changes, blood pressure lowering therapy (e.g., using renin-angiotensin-aldosterone system inhibitors), and improved glycemic control in diabetic kidney disease (DKD) have been the cornerstone of CKD treatment for the last two decades [7–9]. Sodium-glucose cotransporter-2 inhibitors have consistently been demonstrated to lower decline in kidney function and reduce overall risk of major renal outcomes in CKD patients with or without diabetes, and now approved for the treatment of CKD, including DKD [10–15]. In addition, the mineralocorticoid receptor antagonist finerenone has recently been approved for management of DKD and is currently in clinical development for non-diabetic CKD (FIND-CKD; NCT05047263) [16]. However, despite therapeutic advances in CKD, a large proportion of patients still progress to renal failure, highlighting the unmet need for more efficacious therapies that can prevent or reverse progression of the disease.

Animal models of CKD are increasingly important in preclinical target and drug discovery. These models can be broadly grouped into surgical, genetic, and dietary models, and portray different aspects of CKD pathology. Common mouse models of CKD include adenine-supplemented diet-induced (ADI), unilateral urethral obstruction (UUO), and unilateral ischemia-reperfusion injury (uIRI) models. These three models are well-established in experimental CKD research and widely used in preclinical drug screening programs [17–19]. The ADI model is characterized by declining GFR and induction of renal fibrosis and inflammation [20, 21]. In comparison, the UUO model is a surgical model with more rapid onset of renal inflammation and fibrosis [22]. The uIRI model, another surgically induced model, is advantageous for studying the transition from ischemic acute kidney injury to CKD [23]. Importantly, the three models are recognized for their reproducibility and robust kidney inflammatory and fibrotic responses and thus remain instrumental in preclinical target and drug discovery [20, 21, 24–26]. Considering that the three models differ with regards to induction method, disease severity, and clinical translatability, they have individual advantages and limitations and thus different utility in preclinical target and drug discovery [27, 28]. To gain further insight into the complex molecular mechanisms involved in CKD and assist selection of the most relevant mouse model for testing drugs directed at a specific disease mechanism, the present study aimed to compare renal global transcriptome signatures of the ADI, UUO, and uIRI mouse model, respectively.

Materials and Methods

Animals

Male C57BL/6J mice were from Janvier Laboratories (Le Genest Saint Isle, France) and housed in a controlled environment (12 h light/dark cycle, lights on at 3:00 a.m., 21 ± 2°C, humidity 50 ± 10%). Upon arrival, each animal was identified by an implantable subcutaneous microchip (PetID Microchip, E-vet, Haderslev, Denmark). Mice had ad libitum access to tap water and standard chow (3.22 kcal/g, Altromin 1324, Brogaarden, Hoersholm, Denmark), unless otherwise stated. Mice were acclimatized for 2 weeks before study started. Mice were randomized into study groups based on body weight measured on day −3. For an overview of study designs, see Figure 1. All animal experiments were conducted in agreement with internal Gubra bioethical guidelines that are fully compliant with internationally accepted principles for the care and use of laboratory animals.

ADI Model

The experiment utilizing ADI mice was approved by the Danish Animal Experiments Council under license number 2021-15-0201-00915. Twelve-week-old mice received control diet (S9352-E064, Ssniff, Soest, Germany) for 2 days before study started. ADI mice were then switched to an adenine-supplemented diet (0.2% adenine, cat no. S9352-E060, Ssniff, Soest, Germany) for 6 weeks, whereas control mice remained on the control diet. Both ADI and control mice had ad libitum access to tap water and food. Mice were terminated under isoflurane anesthesia by cardiac puncture 6 weeks after study start.

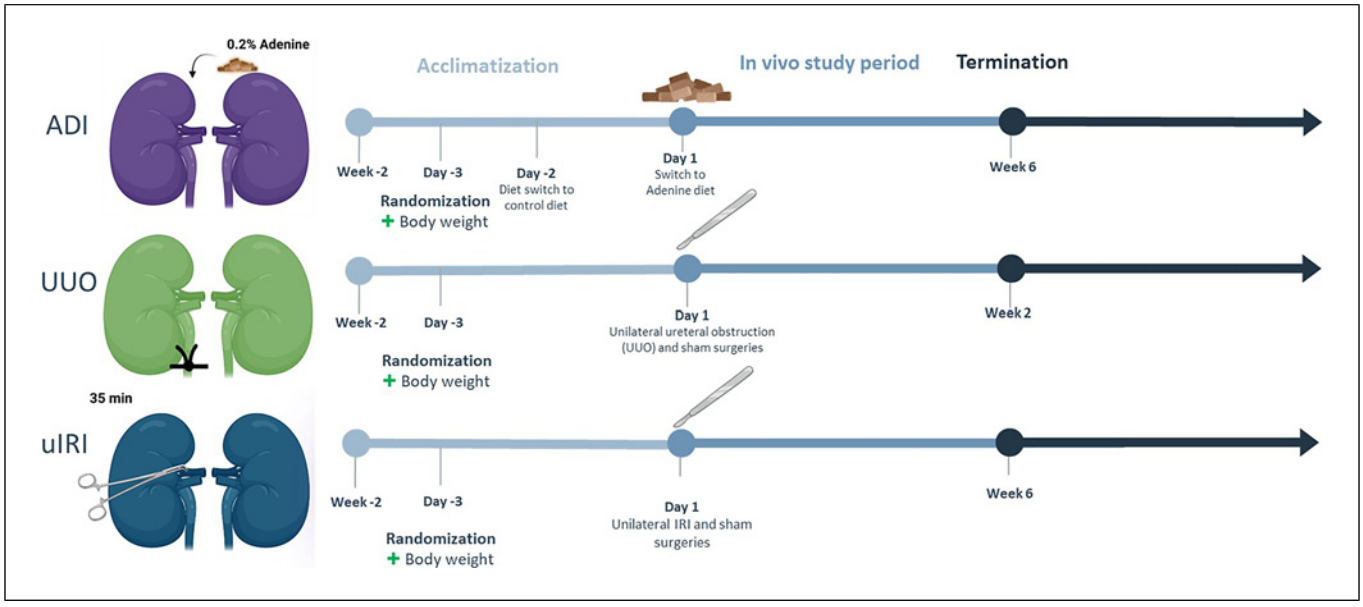

Fig. 1. Outline on ADI, UUO, and uIRI mouse model studies.

Unilateral Ureteral Obstruction Model

The experiment utilizing UUO mice was approved by the Danish Animal Experiments Council under license number 2018-15-0201-01559. UUO was performed in 9-week-old mice. Animals were placed on electrical heating pads under isoflurane anesthesia through the entire surgical procedure. A ventral midline incision was made for localizing the left kidney. The ipsilateral ureter was localized, isolated, and ligated at two locations and cut between the sutures. The linea alba and skin were closed in two layers. Postoperative analgesia (Rimadyl [carprofen]) was administered and continued for three consecutive days post-surgery. Age-matched, sham-operated C57BL/6J mice served as healthy controls. For sham operation, the abdominal cavity was opened, the left kidney and ureter were manipulated but left intact. Anesthesia, analgesia, and opening and closure of the abdominal cavity were conducted as described above. Animals were terminated under isoflurane anesthesia by cardiac puncture 2 weeks after UUO surgery.

uIRI Model

The experiment utilizing uIRI mice was approved by the Danish Animal Experiments Council under license number 2020-15-0201-00623. uIRI was performed in 10-week-old mice. Animals were placed on electrical heating pads under isoflurane anesthesia through the entire surgical procedure. A dorsal midline incision was made through the skin, the muscle above the left kidney was incised and the left kidney hilum was localized and gently dissected free from fat and connective tissue, before a clamp (cat. No. ROBOZ RS-5452, Roboz Surgical Instrument Co., Gaithersburg, MD) was placed to obstruct blood flow. After 35 min the clamp was removed, and the kidney was visually inspected to confirm stabile reperfusion. The muscle and skin were closed in two layers. Post-operative analgesia (Vetergesic [buprenorphine] Orion Pharma, Denmark) and antibiotics (Baytril, [enrofloxacin] Bayer, Germany) were administered and continued for three consecutive days post-surgery. Age-matched, sham-operated C57BL/6J mice served as healthy controls. For sham operations, anesthesia, analgesia and opening and closure of the abdominal cavity was conducted as described above except for omitting the clamp procedure. Animals were terminated 6 weeks post-surgery by cardiac puncture under isoflurane anesthesia.

Blood Biochemistry

Blood samples were centrifuged at 3,000 *g* (4°C) and plasma was collected. Plasma urea was measured using a commercial kit (cat. No. 4460715190, Roche Diagnostics, Mannheim, Germany) on a Cobas™ C-501 autoanalyzer (Roche Diagnostics, Mannheim, Germany).

Tissue Collection

Kidneys were weighed after urine release, and the left renal capsule was removed before splitting the kidney into three transverse sections. The middle section was used for histology (see below). The upper pole of the kidney was split sagitally, snap-frozen in liquid nitrogen and stored at −70°C until further processing for RNA sequencing (see below).

Histology

Samples were fixed overnight in a 10% neutral buffered formalin solution (4% formaldehyde) (Sigma-Aldrich, Denmark) at 4°C, embedded in paraffin and 3 µm sections were cut on a microtome. Immunohistochemistry was performed using standard procedures, as described previously [29, 30]. Briefly, the samples were deparaffinated in xylene and rehydrated in series of graded ethanol. Following antigen retrieval and blocking of endogenous peroxidase activity, the samples were incubated with the primary antibody for collagen 1a1 (Col1a1) (goat anti-type I Collagen 1:100 dilution, Southern Biotech #1310-01, Birmingham,

Table 1. Body weight, kidney weight, and plasma urea levels

	ADI control	ADI	UUO Sham	UUO	uIRI sham	uIRI
n	8	8	8	8	10	10
BW (randomization), g	27.6±0.3	27.6±0.3	23.2±0.4	23.2±0.3	22.9±0.4	24.2±0.3
BW (terminal), g	27.4±0.5	21.1±0.4***	23.6±0.5	23.8±0.5	26.4±0.6	24.5±0.3*
Left kidney weight, mg	167.5±5.1	152.7±5.9	146.5±4.2	148±10.9	156±6.4	63.8±4.1***
Right kidney weight, mg	168.7±5.0	145.2±6.1**	154±4.5	179±5.9*	164±6.5	182.1±5.7
Plasma urea, mmol/L	7.9±0.3	25.6±1.4***	8.9±0.4	9.2±0.6	9.9±0.6	10.7±0.3

All values are ±SEM. *$p < 0.05$, **$p < 0.01$, ***$p < 0.001$ compared to corresponding control group (two-tailed Dunnet's test).

AL) or F4/80 (rat anti-F4/80 [C1:A3-1] 1:200 dilution, cat. No. ab6640, Abcam, Cambridge, United Kingdom). The primary antibody was detected using a polymeric HRP-linker antibody conjugate and visualized using DAB as chromogen. Finally, sections were counterstained in hematoxylin, cover slipped, and scanned under a 20× objective in a Aperio ScanScope AT slide scanner (Leica, Deer Park, IL, USA). Care was taken to ensure that the kidneys were cut using identical anatomical and morphological landmarks on each specimen to reproducibly collect samples at the same anatomical location. Quantitative image analysis was performed using Visiomorph software (Visiopharm, Hørsholm, Denmark). Col1a1 and F4/80 expressions were quantified in the entire renal section. Quantitative levels of Col1a1 and F4/80 were expressed as proportionate (%) area of immunopositive staining.

RNA Sequencing

RNA from snap-frozen kidney cortex samples (20 ± 5 mg per animal) was extracted using a NucleoSpin 8 RNA kit (Macherey-Nagel, Germany) and a vacuum manifold. cDNA library preparation was performed using a NEBNext Ultra II Directional RNA Library Prep Kit for Illumina (E7760L, NEG, Ipswich, MA, USA). The sequencing of cDNA libraries was performed using an NS 500 high Output Kit v2 (75 cycles) (Illumina, San Diego, CA, USA) on an Illumina NextSeq 500 platform (Illumina, San Diego, CA, USA). The gene expression level is displayed as reads per kilobase million, quantifying gene expression from mRNA sequencing data by normalizing for both total read and the number of sequencing reads. Reads were mapped to the GRCm38 v96 Ensembl *Mus musculus* genome using Spliced Transcripts Alignment to a Reference (STAR) v.2.7.0f [31]. The R-package DESeq2 v.1.24.0 was used for differential expression analysis [32]. p values were adjusted using the Benjamini-Hochberg method and genes with an adjusted $p < 0.05$ were considered statistically significantly regulated. Gene set analysis was conducted with the R-package PIANO version 2.0.0 using the Stouffer method [33]. Normalized counts were calculated using the DEseq2 variance stabilizing ratio method for representation using pheatmap v1.0.12 [34]. In pheatmap, the formula:

$$Count_{scaled} = \frac{(Count - \overline{Counts_{row}})}{\sigma(Counts_{row})}$$

was utilized for row-wise scaling of the normalized counts.

Statistical Analysis

Results are presented as mean ± standard error mean (SEM). All data were analyzed using R (v. 3.6.0) and, except for RNAseq data sets, presented using GraphPad Prism software (v. 9.4.1). The two-tailed Dunnett's test was used for significance testing, with a p value less than 0.05 considered statistically significant.

Results

Model-Specific Changes in Body Weight and Blood Biochemistry

Metabolic and biochemical data are summarized in Table 1. Terminal body weight was significantly reduced in ADI and uIRI mice as compared to corresponding controls (ADI $p < 0.001$, uIRI $p < 0.05$). Body weight was unaffected in the UUO model. ADI, but not UUO and uIRI mice, showed significantly increased plasma urea levels ($p < 0.001$; Table 1). uIRI mice demonstrated significantly reduced weight (≥50%) of the affected (left) kidney compared to sham controls ($p < 0.001$). In contrast, UUO mice demonstrated hypertrophy of the unaffected (right) kidney ($p < 0.01$; Table 1). While both left and right kidney mass appeared lowered in ADI mice, only right kidney weight was significantly reduced compared to controls ($p < 0.05$, Table 1).

Model-Specific Differences in Renal Inflammation and Fibrosis Histology

The left kidney in UUO, uIRI, and ADI mice was characterized by quantitative immunohistochemistry (Fig. 2). Fractional (%) area of F4/80 staining, a marker of macrophage infiltration, was significantly increased in all three models as compared to respective controls, most markedly in ADI (12.6 ± 2.2% vs. 1.4 ± 0.1%, $p < 0.001$) and UUO (19.91% vs. 2.1 ± 0.1%, $p < 0.001$) mice

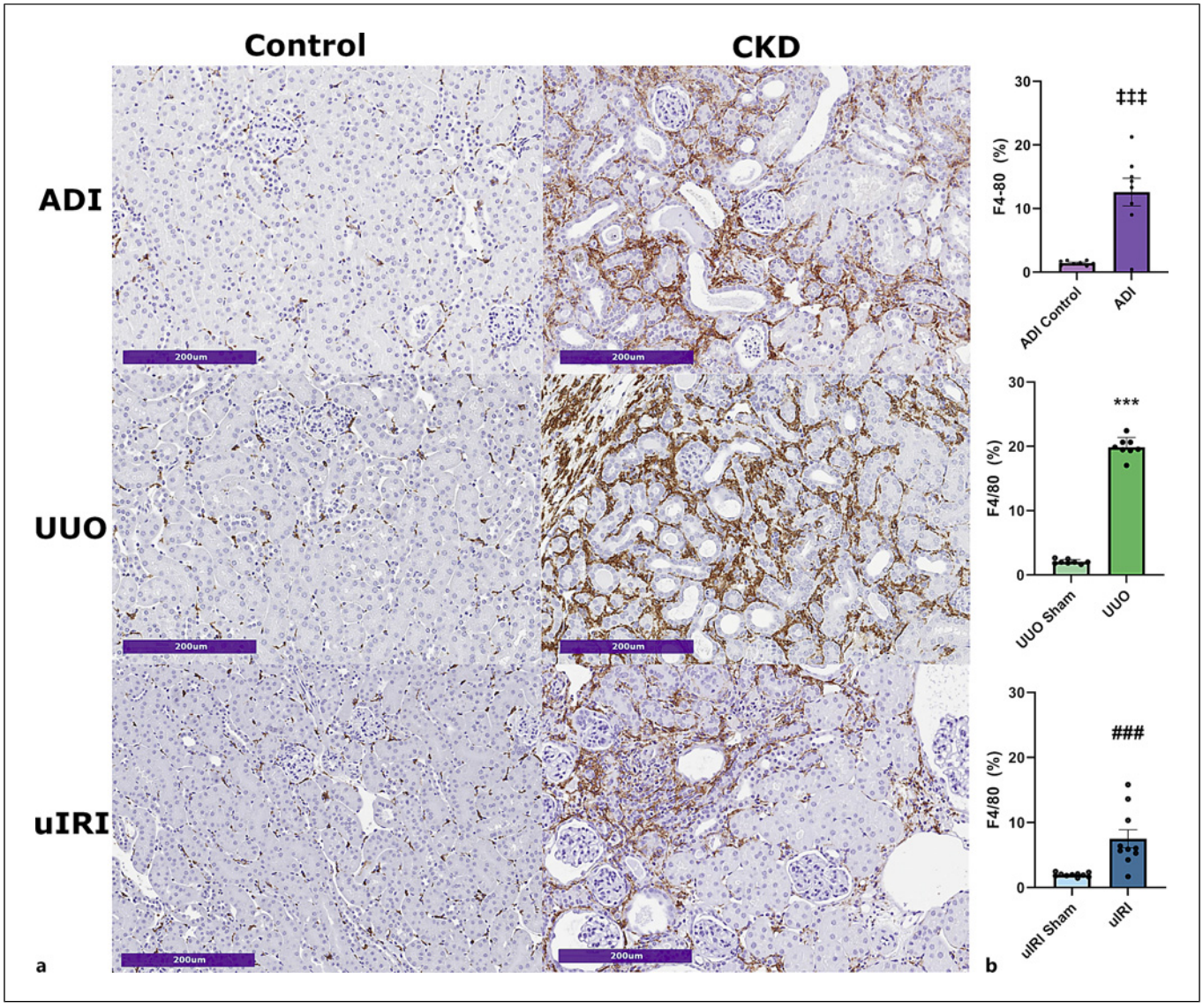

Fig. 2. ADI, UUO, and uIRI mice show increased renal macrophage infiltration (**a**) Representative histological images (left kidney) on F4/80 staining. Scale bar, 200 µm. **b** Relative (%) area of F4/80 staining. All values are ±SEM. $^{‡‡‡}p < 0.001$ compared to ADI control, $^{***}p < 0.001$ compared to UUO sham, $^{###}p < 0.001$ compared to uIRI sham (two-tailed Dunnet's test).

(Fig. 2b). uIRI mice showed a less pronounced increase in %-area of F4/80 staining (7.5 ± 1.4% vs. 2.0 ± 0.1%, $p < 0.001$).

Compared to corresponding controls, ADI and UUO mice showed significant increase in %-area of kidney Col1a1 staining, a marker of fibrosis (ADI, 24.7 ± 0.8% vs. 6.9 ± 0.27%, 3.6 ± 0.1-fold; UUO, 40.3 ± 1.1% vs. 8.7 ± 0.86%, both $p < 0.001$), respectively (Fig. 3b). uIRI mice demonstrated a less robust increase in %-area of Col1a1 (39.6 ± 2.8% vs. 17.7 ± 1.0%, $p < 0.001$).

Shared and Distinct Transcriptome Signatures

A principal component analysis was performed to assess and compare global transcriptome changes in the three models (Fig. 4a). The major variance in the RNAseq data set was explained by the presence of CKD (84%, PC1; model vs. control) and to a lesser degree by the disease induction method applied (6%, PC2), overall indicating extensive gene expression changes in all CKD models compared to corresponding controls. The number of differentially expressed genes (DEGs) were excessive in all

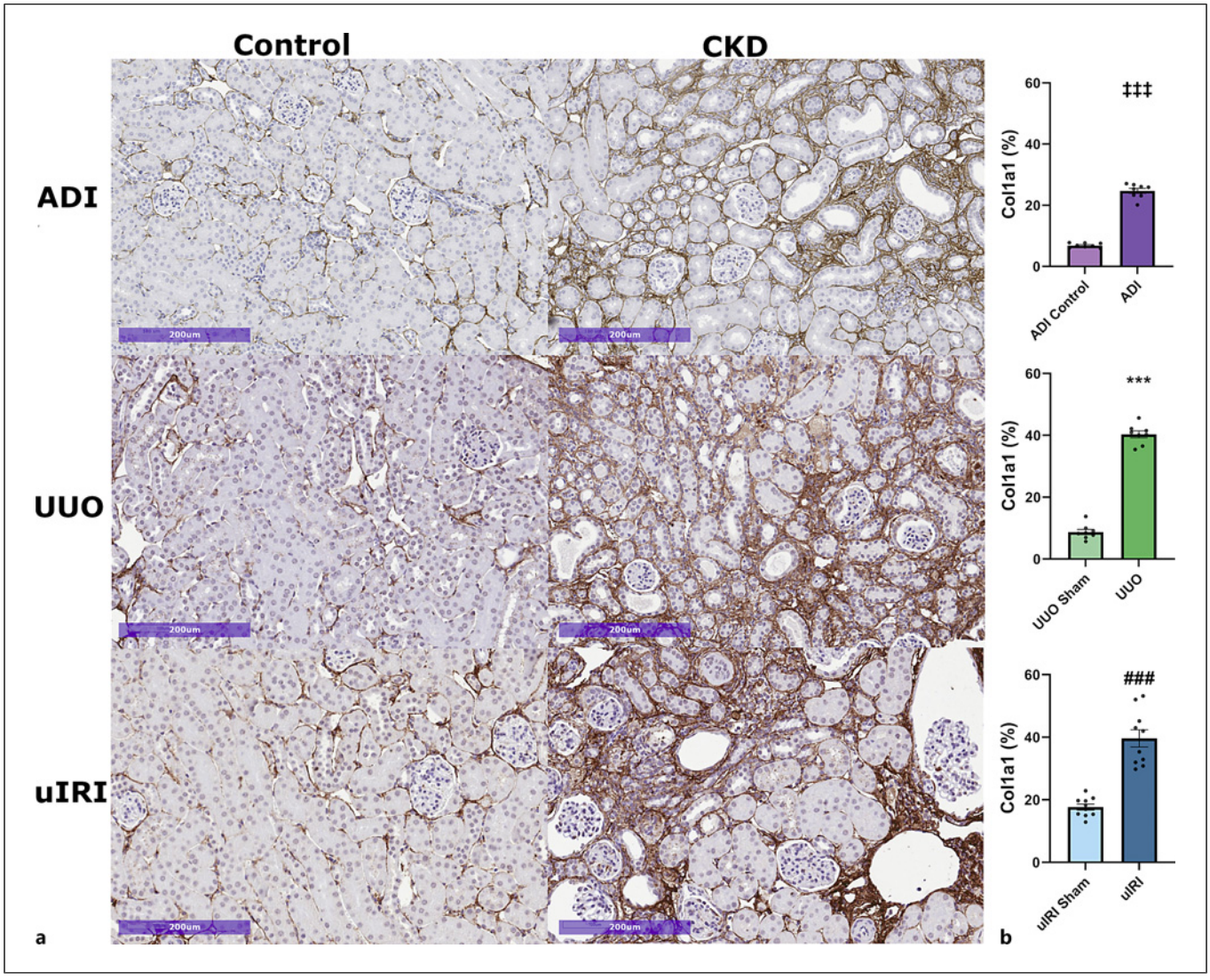

Fig. 3. ADI, UUO, and uIRI models show increased renal fibrosis. **a** Representative histological images of Col1a1 staining in kidney sections. Scale bar, 200 µm. **b** Relative (% area) of Col1a1 staining. All values are ±SEM. $^{‡‡‡}p < 0.001$ compared to ADI control, $^{***}p < 0.001$ compared to UUO sham, $^{###}p < 0.001$ compared to uIRI sham (two-tailed Dunnet's test).

three models (n = 12,236 [uIRI], n = 12,046 [UUO] and n = 11,468 [ADI]), as compared to corresponding controls (Fig. 4b). Notably, the three models shared a large proportion of DEGs, both upregulated (n = 4,578) and downregulated (n = 3,745) (Fig. 4c).

To obtain an overview of perturbed molecular signaling in the three models, a reactome pathway analysis [35] was performed, which indicated highly similar pathway perturbations across models including ECM remodeling and the immune system (online suppl. Fig. S1; for all online suppl. material, see https://doi.org/10.1159/000535918). To assess model-specific signatures, only DEGs unique to each individual model (ADI, n = 1,183, UUO, n = 900 and uIRI, n = 1,860) were included in the analysis (Fig. 5a–c). The top regulated pathways in the ADI model were associated with metabolism and the immune system, with RNA metabolism being the dominant pathway. In contrast, the top regulated pathway for both UUO and uIRI mice was associated with signal transduction, where differences in the type of signal transduction were apparent (online suppl. Fig. S2). The UUO and uIRI mice differed in their second and third

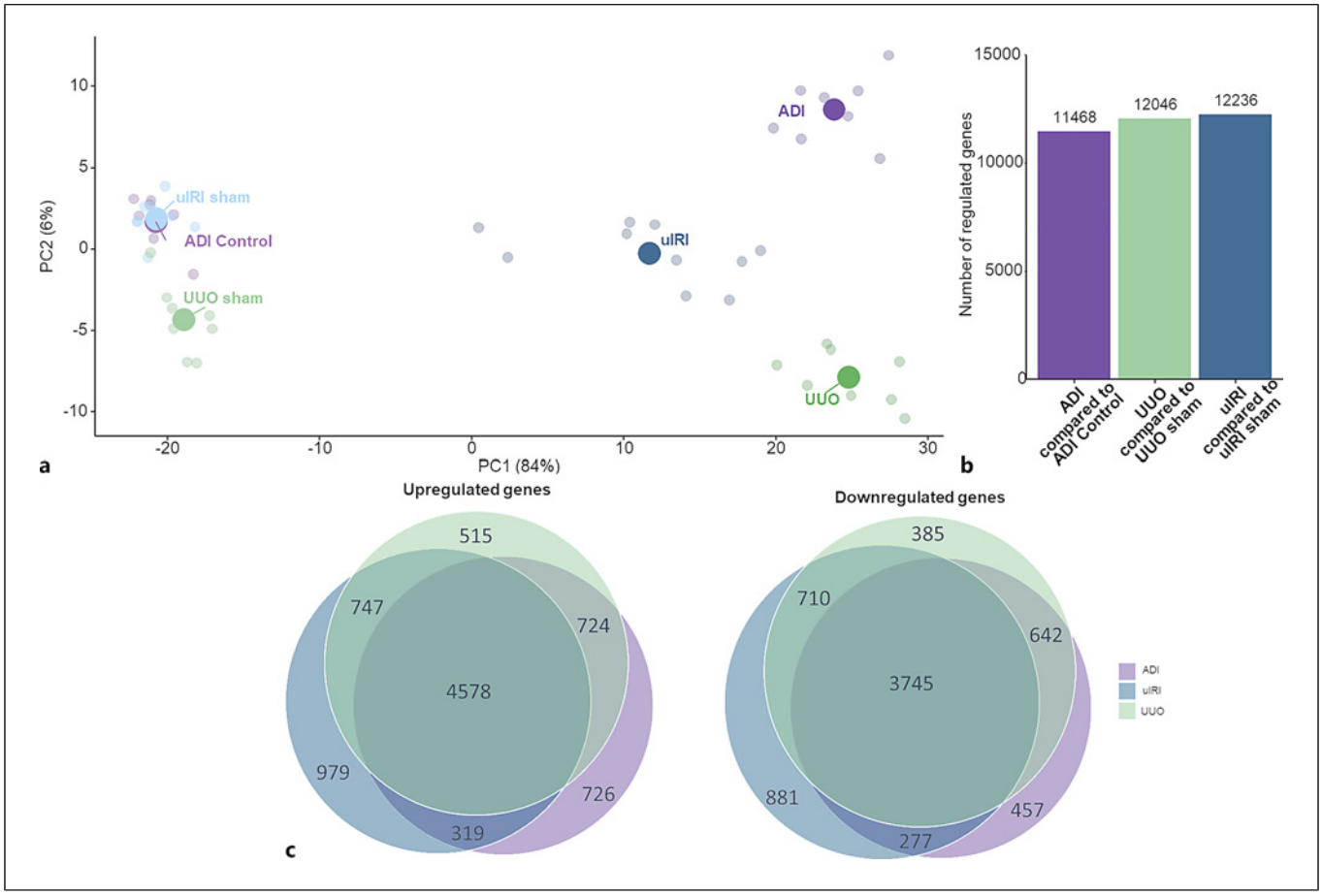

Fig. 4. RNA sequencing analysis reveals distinct model transcriptome signatures, however, with significant overlap between CKD models (**a**) PCA-plot of gene expression changes in top 500 most variable genes. Small dots indicate samples; large dots indicate the center of all samples in a group. **b** Bar plot depicting total regulated genes in the ADI, UUO, and uIRI model compared to corresponding control group. **c** Venn diagrams depicting the overlapping and distinct differentially expressed genes in ADI, uIRI, and UUO mice. PCA, principal component analysis.

most perturbed pathways with UUO mice being associated with ECM organization and hemostasis, while uIRI mice were associated with the neuronal system and transcription.

Considering the clear histological evidence of kidney inflammation and fibrosis in ADI, UUO, and uIRI mice, we first profiled an in-house candidate gene set (online suppl. Table S1) associated with the immune system and ECM (Fig. 6a, b). Most genes involved in fibrogenesis (28 out of 35 genes) showed similar directional change in the three models, with notable upregulation of genes promoting collagen formation (e.g., *Col1a1, Col3a1, Col4a1, Col4a2, Fn1*) and extracellular matrix remodeling (e.g., *Lamc2, Mmp9, Serpine1, Timp1, Vim*). Several genes involved in TGF-β signaling were also upregulated in the three models (e.g., *Grem1, Tgfb1, Tgfb2, Tgfb3, Tgfbr1*). While being regulated in all three models, we detected model-specific directional changes in the expression of a subset of genes involved in TGF-β signaling (i.e., *Avcr1b, Bmpr1a, Bmpr2, Crim1, Eng, Smad4 and Smad5*). For example, *Crim1* was downregulated in ADI mice while being upregulated in uIRI mice and *Smad4* was only upregulated in UUO and uIRI mice.

Immune system-related genes were to a large degree upregulated in all three models (Fig. 6c, d). This applied to, e.g., genes involved in chemokine signaling and immune cell migration (e.g., *Ccl2, Ccr2, Icam1, Vcam1*) as well as monocyte/macrophage markers (e.g., *Il1b, Cd68, Cd86, Mrc1*). Consistent with histological findings, *Adgre1* (F4/80) was also robustly upregulated in all three models.

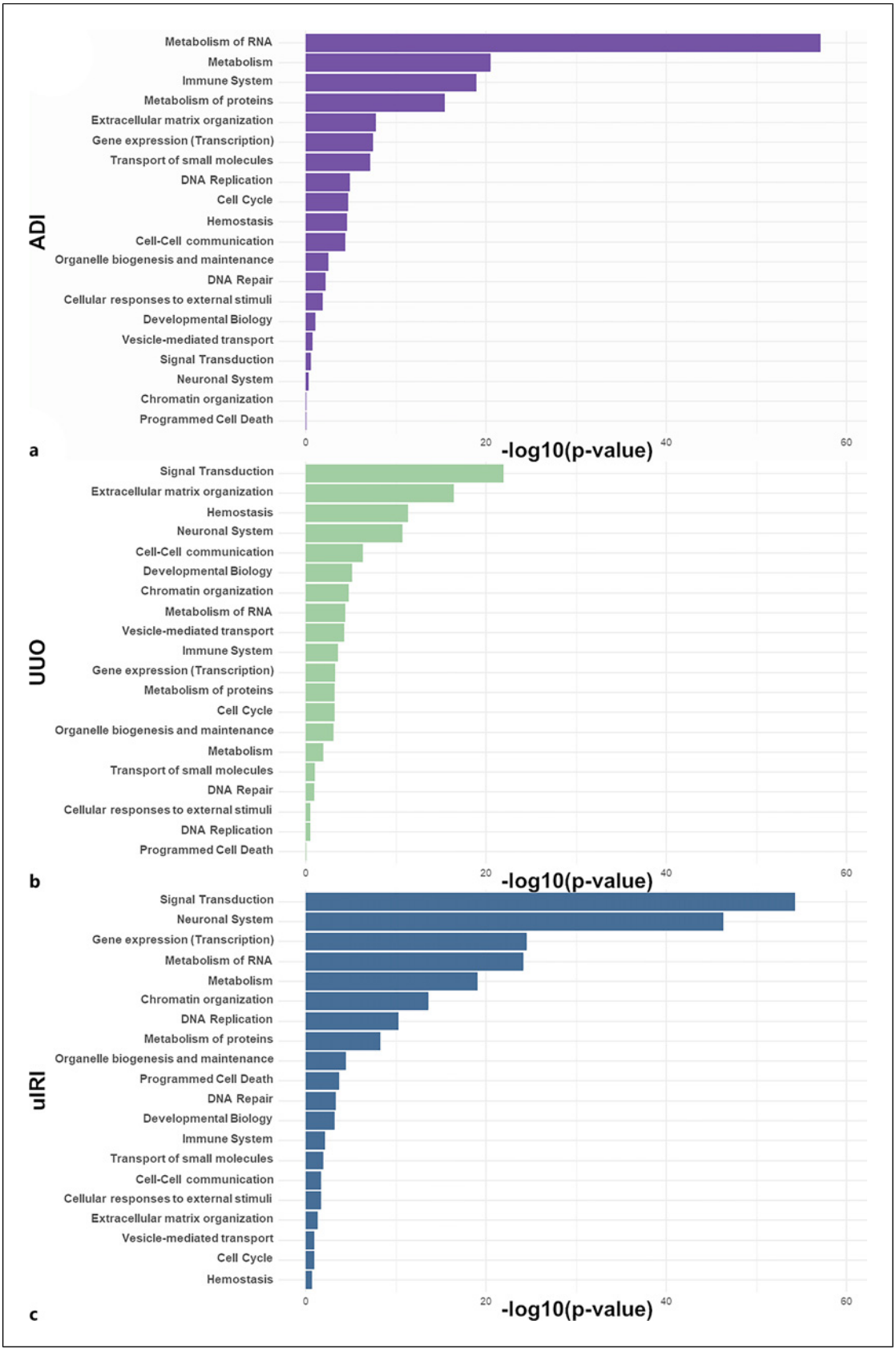

Fig. 5. Reactome pathway analysis of model-specific gene regulations in the ADI, UUO, and uIRI mouse. **a** ADI mice, (**b**) UUO mice, and (**c**) uIRI mice showing inverse log10 *p* values of genes in the top 20 regulated pathways.

In addition, selected gene expression markers of kidney injury [36] were probed in the data set (Fig. 6e, f). Common tubular injury markers such as *Havcr1*, *Lcn2*, and *Spp1* (kidney injury molecule 1, lipocalin 2, and osteopontin) were upregulated in ADI, UUO, and uIRI mice, whereas *Umod* (uromodulin) was downregulated in all models. Compared to ADI and UUO mice, uIRI mice demonstrated inconsistent changes in the renal injury markers *Ambp, Chil1,* and *Igfbp7*.

Mapping Gene Expression Changes in Drug Targets for CKD

Finally, we mapped the expression of molecular targets currently pursued in preclinical and clinical drug development for CKD [2, 37, 38]. Genes were classified according to major biological function and heatmaps were generated to visualize the expression of the target genes across the CKD models as compared to corresponding controls (Fig. 7a, b; online suppl. Table S2). Furthermore, genes which showed model-specific expression patterns as well as molecular targets for current clinical-stage drugs were further explored (Fig. 7c, d). Overall, the ADI, UUO, and uIRI models showed similar patterns of quantitative gene expression changes for drug targets across all functional categories.

Clinical-Stage Drug Targets

All three models demonstrated significant downregulation of *Slc5a2* (encoding sodium-glucose cotransporter-2 inhibitors) and upregulation of *Ednra* (endothelin receptor A) (Fig. 7a, b). *Ednrb* (endothelin receptor B) was upregulated in ADI and downregulated in UUO while seeing no regulation in uIRI. *Nr3c2* and *Glp1r* (mineralocorticoid receptor, glucagon-like peptide-1 receptor), were both upregulated in uIRI mice while being downregulated in UUO mice. *Nr3c2* was significantly downregulated in ADI mice.

Drug Targets Involved in Fibrosis and Inflammation

Most target genes linked to ECM [2] were upregulated in the three CKD models, including those involved in myofibroblast activation (*Gli1*, *Tnc*, *Tnfsf12*), fibroblast proliferation (*Pdgfa*, *Pdgfb*, *Pdgfd*, *Pdgfra*, *Pdgfrb*), matrix metalloproteinases (*Mmp2*, *Mmp9*, *Serpine1*), and TGF-β signaling (*Smad3*, *Tgfb*) (Fig. 7a, b). Similarly, a range of potential drug targets regulating the immune system [2] showed similar directional changes across the models characterized. Most of these genes were upregulated and involved in macrophage-associated pro-inflammatory signaling (*Il1b*, *Il6, Il10*, *Tnf*) and cytokine responses (*Ccl2*, *Nfkb1*, *Nfkb2*). *Ifng* expression was upregulated in UUO and uIRI mice, but unaltered in ADI mice.

Drugs Targets Involved in Tubular Injury and Regeneration

The gene expression changes of molecular targets linked to tubular injury and regeneration [2] were overall similar in ADI, UUO, and uIRI mice, including upregulation of genes associated with apoptosis (*Trp53*), cell dedifferentiation (*Snai1*, *Twist1*) and necrosis (*Ripk3*), downregulation of genes associated with autophagy (*Atg5*, *Map1lc3a*) and cell cycle arrest (*Lamp2*, *Mif*, *Mtor*) and mixed regulation in genes associated with cell senescence (*Cdkn2a*, *Foxo4*, *Myd88*) (Fig. 7a, b). *Ripk1* was not significantly regulated in any model, while *Atg7*, *Bax*, *Egfr*, *Map1lc3b* showed model-specific changes in expression.

Other Mechanisms Pursued in Drug Discovery

The three CKD models showed similar directional changes in the expression of a subset of genes related to angiogenesis (downregulation of *Kdr*, *Vegfa*) and tissue differentiation (upregulation of *Sox9*, *Notch1*, *Notch2*, *Notch3*) (Fig. 7a, b). Model-specific transcriptional changes were observed for other genes involved in angiogenesis (*Flt1*), tissue differentiation (*Ctnnb1*, *Gli2*, *Shh*, *Ptch1*), and peptide receptor signaling (*Gipr* [38]).

Discussion

We here report the first head-to-head comparative study of kidney histopathological and global gene expression changes in 3 widely used mouse models of CKD, including the ADI, UUO, and uIRI model. While the three models demonstrated different severity of kidney inflammation and fibrosis, our comprehensive RNAseq and bioinformatics analysis indicated remarkably overlapping renal transcriptome signatures. All three models can therefore inform about renal molecular signaling implicated in CKD and selection of the relevant mouse model in preclinical target and drug discovery will depend on the specific study design, which should consider drug/target mode of action, model disease severity and study cost-effectiveness.

Our histomorphometric analysis confirmed and extended previous histological studies in ADI, UUO, and uIRI mice [39–43]. Overall, the UUO model showed the

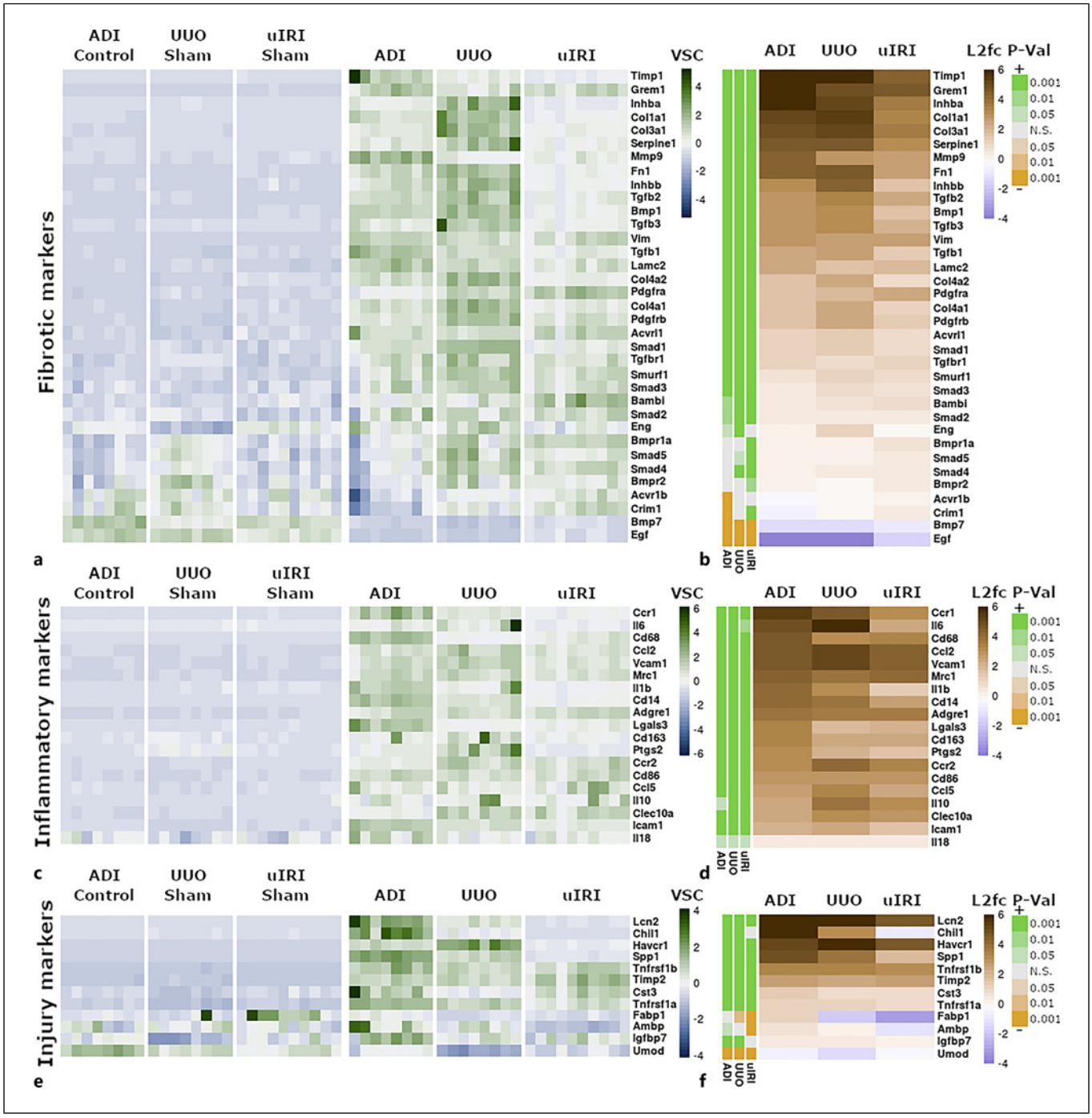

Fig. 6. a Gene expression (normalized counts) of fibrotic markers in all models and all controls scaled row-wise, with squares representing individual animals (n = 8 for ADI, UUO, n = 10 for uIRI). **b** Log2-fold change in gene expression of fibrotic markers from controls to CKD animals. Rows are unscaled. Also shown are p values representing directionality of regulation for all three models. **c** Gene expression (normalized counts) of inflammatory markers in all models and all controls scaled row-wise, with squares representing individual animals. **d** Log2-fold change in gene expression of inflammatory markers from controls to CKD animals. Rows are unscaled. Also shown are p values representing directionality of regulation for all three models. **e** Gene expression (normalized counts) of kidney injury markers in all models and all controls scaled row-wise, with squares representing individual animals. **f** Log2-fold change in gene expression of injury markers from controls to CKD animals. Rows are unscaled. Also shown are p values representing directionality of regulation for all three models.

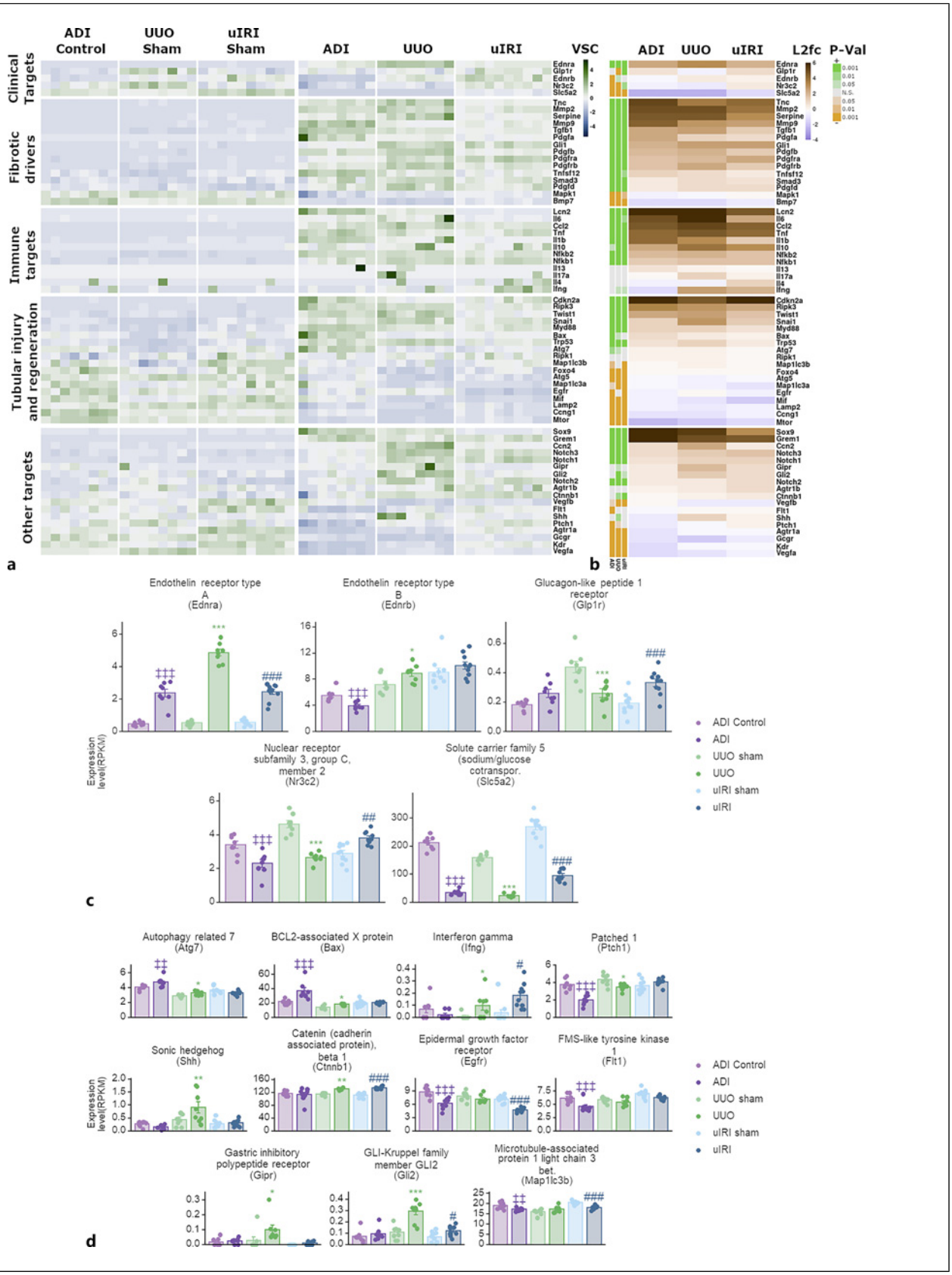

(For legend see next page.)

most advanced renal fibrosis and inflammation. Kidney fibrosis was also prominent in uIRI mice while demonstrating a relatively mild inflammatory response. In comparison, the ADI mouse model developed milder kidney fibrosis with moderate-grade inflammation. While previous kidney transcriptomic studies have been reported in the UUO and uIRI mouse [44, 45], similar information is lacking for the ADI mouse model. Also, no head-to-head comparison of the renal transcriptome changes in these 3 mouse models has been performed. While the models were clearly separated based on different degree of inflammatory and fibrotic injury, overall kidney transcriptome signatures were remarkably similar in these common mouse models of CKD. A shared characteristic in all three models was a very high number of differentially expressed genes involving almost half of the kidney global transcriptome. Collectively, the genome-wide responses appeared to a large degree independent of the individual CKD induction method applied, indicating that the three model paradigms all promote considerable and widespread alterations in renal molecular signaling.

The three models were investigated for model-specific transcriptome changes. Our analysis indicated that the three models to a minor degree differed in gene expression events associated with wide range of kidney functional domains, including metabolism, ECM organization, immune system as well as hemostatic and neuronal signaling pathways. While the models were clearly distinguished based on fibrosis severity, our RNAseq data suggest relatively comparable profibrogenic activity in the three models based on selected fibrosis markers. It should be emphasized that changes in gene expression do not always correlate with changes in protein levels, given the vast range of post-translational regulatory mechanisms that can influence the expression and turnover rate of the corresponding protein.

For all models, the most conspicuous gene expression changes were linked to transcriptional programs indicative of enhanced fibrogenesis and reduced clearance of collagen fibers, thus favoring fibrosis progression. In agreement with previous studies in ADI, UUO, and uIRI mice [46–52], we observed a marked upregulation of *Col1a1, Col3a1 Col4a1, Col4a2*, and *Fn1* across the models. Similar findings have been reported in CKD patients [53]. Also consistent with regulation of profibrotic TGF-β signaling in human CKD [54], genes associated with TGF-β signaling (e.g., *Bmpr2*, *Mmp9*, *Tgfb1*, *Timp1, Tgfb1r*) were significantly upregulated in all three models, further supporting that TGF-β signaling is critical in fibrotic kidney injury and thus an attractive drug target in CKD [26, 41, 47, 55–59]. Few ECM-related genes were downregulated, notably *Bmp7* and *Egf*. These two genes are involved in cellular dedifferentiation and also reported downregulated in human CKD, a mechanism thought to favor fibrosis [60, 61].

As for fibrosis, the models showed comparable changes in gene expression markers of inflammation, indicating a broad inflammatory response involving marked upregulation of pro-inflammatory signaling and recruitment of immune cells, notably macrophages and T-cells. These regulatory events were supported by previous preclinical [26, 48, 50, 52, 62, 63] and clinical [64–67] studies.

Kidney damage in the three CKD models was further supported by significant regulation of gene expression markers of acute and chronic renal injury. In agreement with previous studies in ADI, UUO, and uIRI mice, we observed a marked upregulation of key markers of kidney injury, including *Havcr1* [47, 48, 68], *Lcn2* [68–70], and *Spp1* [40, 71]. These genes have been demonstrated to play an important role in renal regeneration and inflammatory responses in preclinical studies [72–75] and also implicated in human CKD pathogenesis [76, 77].

Given the applicability of the ADI, UUO, and uIRI mouse models in preclinical target and drug discovery, we performed a comparative analysis of renal molecular targets currently pursued in preclinical and clinical drug discovery. Targets selected were classified into four major

Fig. 7. Gene expression analysis of current and putative drug targets showed key differences in regulation between models. **a** Heatmap of gene expression (Variance corrected counts) of CKD drug targets, scaled row-wise, with squares representing individual animals (n = 8 for ADI, UUO, n = 10 for uIRI). Drug targets are separated into several groups, based on putative function [2, 37, 38]. **b** Log2-fold change in gene expression of CKD drug targets from controls to disease-model animals. Rows are unscaled. Also shown are p values representing directionality of regulation for all three models. Drug targets are separated into several groups, based on putative function. **c** Expression levels of current drug targets are shown as mean ± SEM RPKM values. **d** Expression levels of targets with differences in regulation directionality are shown as mean ± SEM RPKM values. $^{*}p < 0.05$, $^{**}p < 0.01$, $^{***}p < 0.001$ compared to UUO sham. $^{‡‡}p < 0.01$, $^{‡‡‡}p < 0.001$ compared to ADI control. $^{\#}p < 0.05$, $^{\#\#}p < 0.01$, $^{\#\#\#}p < 0.001$ compared to uIRI sham. RPKM, reads per kilobase million.

functional categories, i.e., fibrosis, inflammation, tubular injury and regeneration [2]. As for other gene sets applied in the present study, the models demonstrated a significant overlap in the regulation of genes encoding renal targets considered relevant in CKD therapy. One exception was *Ifng* not being regulated in ADI mice. Others have reported upregulated *Ifng* expression in ADI mice [68], possibly reflecting the shorter feeding and study duration of the referenced study. Future studies should aim to investigate a potentially differential role of *Ifng* in the three CKD models.

Interestingly, a range of genes encoding drug targets pursued in clinical trials [37] were regulated differently in the models, including genes involved in Sonic hedgehog signaling (*Gli2, Ptch1, Shh*) and angiogenesis (*Flt1*). Accordingly, *Gli2* and *Shh* were upregulated and *Ptch1* downregulated in UUO mice, corroborating previous studies in this model [78, 79]. Upregulation of renal *Gli2* expression, albeit with unchanged *Ptch1* expression, has been reported in CKD patients [80]. Both *Ptch1* and *Flt1* were downregulated in ADI mice. Previous studies have linked increased levels of soluble FLT1 (Fms Related Receptor Tyrosine Kinase 1) to increased proteinuria in humans [81]. Whether the decrease in *Flt1* expression reflects a lower level of soluble *Flt1* in the murine ADI model must await further studies. Genes encoding receptors targeted by drugs in current clinical development for CKD (*Ednrb, Glp1r, Nr3c2*) showed model-specific regulation. Previous studies in ADI and UUO mice have reported non-significant regulation of *Ednrb,* contrasting the current study [82]. Likewise, lowered *Nr3c2* expression in UUO mice contrasts the finding of upregulated *Nr3cs* expression in a previous study [83]. A peptide receptor with therapeutic potential in metabolic diseases (*Gipr* [38]) was only upregulated in the UUO model. Collectively, the clinically relevant targets for CKD showed different directionality in the ADI, UUO, and uIRI models, which should be considered when probing test compounds for therapeutic effects in these models.

While our study highlights markedly overlapping transcriptome signatures in ADI, UUO, and uIRI mice, other features of the three models are important to consider. For example, establishing the ADI model does not require surgical skills but progression of CKD is slow in the model. While UUO and uIRI mice show normal eGFR due to compensatory upregulation of contralateral kidney function [84], ADI mice have reduced eGFR [20, 21], thus enabling the use of a clinical functional endpoint in this model. Although the UUO and uIRI mouse models are both surgically induced, the UUO model has the advantage of accelerated development of kidney fibrosis and inflammation, thus more applicable in drug screening programs. It should, however, be noted that the UUO model does not reflect the natural history of CKD. In contrast, the uIRI model is considered recapitulating human renal ischemic insults leading to acute kidney injury and thus preferred for testing drugs targeting mechanisms leading to oxidative cell damage [24–26].

Certain study limitations apply. For example, we only characterized the models at a single time point after CKD induction. Hence, we cannot exclude further model-specific transcriptional responses at other timepoints. This aspect must be addressed in future longitudinal studies aiming to further inform about optimal study design and applicable endpoints to assess for potential nephroprotective drug action in each CKD model. The timepoints investigated in the 3 individual mouse models reflect CKD at a relatively advanced histological stage, in particular with regards to the UUO and uIRI model. The differential CKD model phenotypes, including disease severity, should be taken into account when interpreting commonalities and distinct changes in the expression of current clinical CKD molecular targets. Given the presence of significant kidney inflammation and fibrosis in the three models evaluated, this could suggest that differential expression of several clinically relevant drug targets reflect their involvement in advanced CKD, which may be targeted to prevent further progression or ultimately reverse the disease. Overall, these models are therefore most applicable in disease intervention studies rather than prophylactic treatment paradigms. Also, the current study only involved young, male mice. Recent consensus guidelines from the International Society of Nephrology recommend also investigating the effect of sex and aging in murine models of CKD [85]. In addition, quantitative gene expression changes do not necessarily predict similar changes in the expression of the corresponding protein product. In line with this, relative increases in the expression of *Adgre1* and *Col1a1* mRNA were more pronounced than the corresponding changes in F4/80 and Col1a1 immunoreactivity. Therefore, proteomics studies must be performed to further delineate shared and distinct molecular signatures in the models. Finally, while the present study did not aim to characterize treatment responses in the three models, future intervention studies could serve to differentiate transcriptome responses in these three models with the aim to further guide preclinical target and drug discovery studies using these models.

In conclusion, our study reveals a large overlap in kidney transcriptome signatures in the ADI, UUO, and uIRI models of CKD. The commonalities in global gene expression responses suggest that the three models are

most likely equally applicable in preclinical CKD research. However, the different induction methodologies and model-specific changes in certain genes important in CKD pathogenesis highlight that the three models have individual advantages and limitations in preclinical target and drug discovery for CKD. The model of interest should therefore preferentially be selected based on considerations on drug target, mode of action, applicable endpoints, and feasibility of the CKD induction method applied.

Statement of Ethics

The Danish Animal Experiments Inspectorate approved all experiments (license No. 2020-15-0201-00623, 2018-15-0201-01559, and 2021-15-0201-00915), which were conducted using internationally accepted principles of laboratory animals.

Conflict of Interest Statement

Adam B. Mastrand-Jørgensen, Frederikke Emilie Sembach, Stine Thorhauge Bak, Maria Ougaard, Mikkel Christensen-Dalsgaard., Martin Rønn Madsen., Ditte Marie Jensen., Sebastian Møller Nguyen Heimbürger, Henrik H. Hansen., Michael Christensen, and Louise S. Dalbøge are employed by Gubra and shareholders in Gubra. Mette Viberg Østergaard and Thomas Secher were employed by Gubra and were presently employed by Novo Nordisk A/S. Lisbeth N. Fink was employed by Gubra and was presently employed by Ferring Pharmaceuticals A/S. No other potential conflicts of interest were reported.

Funding Sources

This research received funding from the Innovation Fund Denmark (Grant Number 2040-00034B).

Author Contributions

Conceptualization and writing-original draft preparation: Adam B. Mastrand-Jørgensen, Louise S. Dalbøge, Frederikke Emilie Sembach, and Henrik H. Hansen; methodology: Stine Thorhauge Bak, Maria Ougaard, Mikkel Christensen-Dalsgaard., Martin Rønn Madsen, Ditte Marie Jensen., Thomas Secher, Lisbeth N. Fink, and Mette Viberg Østergaard; formal analysis: Adam B. Mastrand-Jørgensen, S.T.B, Ditte Marie Jensen, and Thomas Secher; data curation: Adam B. Mastrand-Jørgensen, Martin Rønn Madsen, Mikkel Christensen-Dalsgaard; writing-review and editing: Adam B. Mastrand-Jørgensen, Louise S. Dalbøge, Frederikke Emilie Sembach, Henrik H. Hansen, Stine Thorhauge Bak, Maria Ougaard, Mikkel Christensen-Dalsgaard., Martin Rønn Madsen, Ditte Marie Jensen, Sebastian Møller Nguyen Heimbürger, Thomas Secher, Lisbeth N. Fink, and Mette Viberg Østergaard, Ditte Marie Jensen, and Mikkel Christensen; visualization: Adam B. Mastrand-Jørgensen; supervision: Louise S. Dalbøge, and Henrik H. Hansen. All authors have read and agreed to the final version of the manuscript.

Data Availability Statement

The data that support the findings of this study are not publicly available due to samples obtained from clinical research program where restrictions may apply but are available from the corresponding author (L.S.D.) upon reasonable request.

References

1 Stevens PE, Levin A; Kidney Disease: Improving Global Outcomes Chronic Kidney Disease Guideline Development Work Group Members. Evaluation and management of chronic kidney disease: synopsis of the kidney disease: improving global outcomes 2012 clinical practice guideline. Ann Intern Med. 2013;158(11):825–30.
2 Ruiz-Ortega M, Rayego-Mateos S, Lamas S, Ortiz A, Rodrigues-Diez RR. Targeting the progression of chronic kidney disease. Nat Rev Nephrol. 2020;16(5):269–88.
3 Kovesdy CP. Epidemiology of chronic kidney disease: an update 2022. Kidney Int Suppl. 2022;12(1):7–11.
4 GBD 2019 Diseases and Injuries Collaborators; Abbas KM, Abbasi-Kangevari M, Abd-Allah F, Abdelalim A, Abdollahi M, et al. Global burden of 369 diseases and injuries in 204 countries and territories, 1990–2019: a systematic analysis for the Global Burden of Disease Study 2019. Lancet. 2020;396(10258):1204–22.
5 Romagnani P, Remuzzi G, Glassock R, Levin A, Jager KJ, Tonelli M, et al. Chronic kidney disease. Nat Rev Dis Prim. 2017;3:17088.
6 GBD 2015 Disease and Injury Incidence and Prevalence Collaborators; Allen C, Arora M, Barber RM, Brown A, Carter A, et al. Global, regional, and national incidence, prevalence, and years lived with disability for 310 diseases and injuries, 1990–2015: a systematic analysis for the Global Burden of Disease Study 2015. Lancet. 2016;388(10053):1545–602.
7 Kelly JT, Su G, Zhang L, Qin X, Marshall S, González-Ortiz A, et al. Modifiable lifestyle factors for primary prevention of CKD: a systematic review and meta-analysis. J Am Soc Nephrol. 2021;32(1):239–53.
8 Xie X, Liu Y, Perkovic V, Li X, Ninomiya T, Hou W, et al. Renin-angiotensin system inhibitors and kidney and cardiovascular outcomes in patients with CKD: a bayesian network meta-analysis of randomized clinical trials. Am J Kidney Dis. 2016;67(5):728–41.
9 Kidney KDIGO. Disease: improving Global Outcomes (KDIGO) CKD Work Group. KDIGO 2012 clinical practice guideline for the evaluation and management of chronic kidney disease. Kidney Int Suppl. 2013;3:1–150.
10 Perkovic V, Jardine MJ, Neal B, Bompoint S, Heerspink HJL, Charytan DM, et al. Canagliflozin and renal outcomes in type 2 diabetes and nephropathy. N Engl J Med. 2019;380(24):2295–306.
11 Heerspink HJL, Stefánsson BV, Correa-Rotter R, Chertow GM, Greene T, Hou FF, et al. Dapagliflozin in patients with chronic kidney disease. N Engl J Med. 2020;383(15):1436–46.
12 Hill C, Spring S. Empagliflozin and progression of kidney disease in type 2 diabetes. N Engl J Med. 2016;375(18):1799–802.
13 Cannon CP, Pratley R, Dagogo-Jack S, Mancuso J, Huyck S, Masiukiewicz U, et al. Cardiovascular outcomes with ertugliflozin in type 2 diabetes. N Engl J Med. 2020;383(15):1425–35.

14 The EMPA-KIDNEY Collaborative Group, Herrington WG, Staplin N, Wanner C, Green JB, Hauske SJ, et al. Empagliflozin in patients with chronic kidney disease. N Engl J Med. 2023;388(2):117–27.
15 Jafar TH. FDA approval of dapagliflozin for chronic kidney disease: a remarkable achievement? Lancet. 2021;398(10297):283–4.
16 Frampton JE. Finerenone: first approval. Drugs. 2021;81(15):1787–94.
17 Shiva N, Sharma N, Kulkarni YA, Mulay SR, Gaikwad AB. Renal ischemia/reperfusion injury: an insight on in vitro and in vivo models. Life Sci. 2020;256:117860.
18 Martínez-Klimova E, Aparicio-Trejo OE, Tapia E, Pedraza-Chaverri J. Unilateral ureteral obstruction as a model to investigate fibrosis-attenuating treatments. Biomolecules. 2019;9(4):141.
19 Djudjaj S, Boor P. Cellular and molecular mechanisms of kidney fibrosis. Mol Aspects Med. 2019;65(June):16–36.
20 Berru FN, Gray SE, Thome T, Kumar RA, Salyers ZR, Coleman M, et al. Chronic kidney disease exacerbates ischemic limb myopathy in mice via altered mitochondrial energetics. Sci Rep. 2019;9(1):15547–15.
21 Thome T, Kumar RA, Burke SK, Khattri RB, Salyers ZR, Kelley RC, et al. Impaired muscle mitochondrial energetics is associated with uremic metabolite accumulation in chronic kidney disease. JCI Insight. 2020;6(1):e139826.
22 Chevalier RL, Forbes MS, Thornhill BA. Ureteral obstruction as a model of renal interstitial fibrosis and obstructive nephropathy. Kidney Int. 2009;75(11):1145–52.
23 Coca SG, Singanamala S, Parikh CR. Chronic kidney disease after acute kidney injury: a systematic review and meta-analysis. Kidney Int. 2012;81(5):442–8.
24 Buvall L, Menzies RI, Williams J, Woollard KJ, Kumar C, Granqvist AB, et al. Selecting the right therapeutic target for kidney disease. Front Pharmacol. 2022;13(November):971065–5.
25 Eddy AA, López-Guisa JM, Okamura DM, Yamaguchi I. Investigating mechanisms of chronic kidney disease in mouse models. Pediatr Nephrol. 2012;27(8):1233–47.
26 Jia T, Olauson H, Lindberg K, Amin R, Edvardsson K, Lindholm B, et al. A novel model of adenine-induced tubulointerstitial nephropathy in mice. BMC Nephrol. 2013;14(1):116.
27 Rabe M, Schaefer F. Non-transgenic mouse models of kidney disease. Nephron. 2016;133(1):53–61.
28 Nogueira A, Pires MJ, Oliveira PA. Pathophysiological mechanisms of renal fibrosis: a review of animal models and therapeutic strategies. Vivo. 2017;31(1):1–22.
29 Østergaard MV, Sembach FE, Skytte JL, Roostalu U, Secher T, Overgaard A, et al. Automated image analyses of glomerular hypertrophy in a mouse model of diabetic nephropathy. Kidney360. 2020;1(6):469–79.
30 Sembach FE, Fink LN, Johansen T, Boland BB, Secher T, Thrane ST, et al. Impact of sex on diabetic nephropathy and the renal transcriptome in UNx db/db C57BLKS mice. Physiol Rep. 2019;7(24):e14333–9.
31 Dobin A, Davis CA, Schlesinger F, Drenkow J, Zaleski C, Jha S, et al. STAR: ultrafast universal RNA-seq aligner. Bioinformatics. 2013;29(1):15–21.
32 Love MI, Huber W, Anders S. Moderated estimation of fold change and dispersion for RNA-seq data with DESeq2. Genome Biol. 2014;15(12):550–21.
33 Väremo L, Nielsen J, Nookaew I. Enriching the gene set analysis of genome-wide data by incorporating directionality of gene expression and combining statistical hypotheses and methods. Nucleic Acids Res. 2013;41(8):4378–91.
34 Kolde R. Pheatmap. 2019. Available from: https://cran.r-project.org/package=pheatmap.
35 Gillespie M, Jassal B, Stephan R, Milacic M, Rothfels K, Senff-Ribeiro A, et al. The reactome pathway knowledgebase 2022. Nucleic Acids Res. 2022;50(D1):D687–92.
36 Zhang WR, Parikh CR. Biomarkers of acute and chronic kidney disease. Annu Rev Physiol. 2019;81:309–33.
37 Mende CW. Chronic kidney disease and SGLT2 inhibitors: a review of the evolving treatment landscape. Adv Ther. 2022;39(1):148–64.
38 Bulum T. Nephroprotective properties of the glucose-dependent insulinotropic polypeptide (GIP) and glucagon-like peptide-1 (GLP-1) receptor agonists. Biomedicines. 2022;10(10):2586.
39 De Lorenzo SB, Vrieze AM, Johnson RA, Lien KR, Nath KA, Garovic VD, et al. KLF11 deficiency enhances chemokine generation and fibrosis in murine unilateral ureteral obstruction. PLoS One. 2022;17(4):e0266454–17.
40 Li H, Cai H, Deng J, Tu X, Sun Y, Huang Z, et al. TGF-β-mediated upregulation of Sox9 in fibroblast promotes renal fibrosis. Biochim Biophys Acta Mol Basis Dis. 2018;1864(2):520–32.
41 Wei L, Yu Z, Liu L, Zhou Y, Bai X, Wang L, et al. Integrated analysis of the CircRNA-based ceRNA network in renal fibrosis induced by ischemia reperfusion injury. Front Genet. 2021;12(February):793182–14.
42 Tamura M, Aizawa R, Hori M, Ozaki H. Progressive renal dysfunction and macrophage infiltration in interstitial fibrosis in an adenine-induced tubulointerstitial nephritis mouse model. Histochem Cell Biol. 2009;131(4):483–90.
43 Moonen L, Geryl H, D'Haese PC, Vervaet BA. Short-term dexamethasone treatment transiently, but not permanently, attenuates fibrosis after acute-to-chronic kidney injury. BMC Nephrol. 2018;19(1):343–12.
44 Liu J, Kumar S, Dolzhenko E, Alvarado GF, Guo J, Lu C, et al. Molecular characterization of the transition from acute to chronic kidney injury following ischemia/reperfusion. JCI Insight. 2017;2(18):e94716–18.
45 Arvaniti E, Moulos P, Vakrakou A, Chatziantoniou C, Chadjichristos C, Kavvadas P, et al. Whole-transcriptome analysis of UUO mouse model of renal fibrosis reveals new molecular players in kidney diseases. Sci Rep. 2016;6(December 2015):26235–16.
46 de Frutos S, Luengo A, García-Jérez A, Hatem-Vaquero M, Griera M, O'Valle F, et al. Chronic kidney disease induced by an adenine rich diet upregulates integrin linked kinase (ILK) and its depletion prevents the disease progression. Biochim Biophys Acta Mol Basis Dis. 2019;1865(6):1284–97.
47 Loganathan K, Said ES, Winterrowd E, Orebrand M, He L, Vanlandewijck M, et al. Angiopoietin-1 deficiency increases renal capillary rarefaction and tubulointerstitial fibrosis in mice. PLoS One. 2018;13(1):1–18.
48 Chen JH, Wu CH, Jheng JR, Chao CT, Huang JW, Hung KY, Liu SH, et al. The down-regulation of XBP1, an unfolded protein response effector, promotes acute kidney injury to chronic kidney disease transition. J Biomed Sci. 2022;29(1):46–22.
49 Wang B, Koh P, Winbanks C, Coughlan MT, McClelland A, Watson A, et al. miR-200a Prevents renal fibrogenesis through repression of TGF-β2 expression. Diabetes. 2011;60(1):280–7.
50 Yi H, Huang C, Shi Y, Cao Q, Chen J, Chen XM, et al. Metformin attenuates renal fibrosis in a mouse model of adenine-induced renal injury through inhibiting TGF-β1 signaling pathways. Front Cell Dev Biol. 2021;9(February):1–10.
51 Yang L, Besschetnova TY, Brooks CR, Shah JV, Bonventre JV. Epithelial cell cycle arrest in G2/M mediates kidney fibrosis after injury. Nat Med. 2010;16(5):535–143.
52 Waasdorp M, de Rooij DM, Florquin S, Duitman JW, Spek CA. Protease-activated receptor-1 contributes to renal injury and interstitial fibrosis during chronic obstructive nephropathy. J Cell Mol Med. 2019;23(2):1268–79.
53 Huang A, Guo G, Yu Y, Yao L. The roles of collagen in chronic kidney disease and vascular calcification. J Mol Med. 2021;99(1):75–92.
54 Chen L, Yang T, Lu DW, Zhao H, Feng YL, Chen H, et al. Central role of dysregulation of TGF-β/Smad in CKD progression and potential targets of its treatment. Biomed Pharmacother. 2018;101:670–81.
55 Sánchez-Jaramillo EA, Gasca-Lozano LE, Vera-Cruz JM, Hernández-Ortega LD, Gurrola-Díaz CM, Bastidas-Ramírez BE, et al. Nanoparticles formulation improves the antifibrogenic effect of quercetin on an adenine-induced model of chronic kidney disease. Int J Mol Sci. 2022;23(10):5392–17.
56 Bai Y, Wang W, Yin P, Gao J, Na L, Sun Y, et al. Ruxolitinib alleviates renal interstitial fibrosis in UUO mice. Int J Biol Sci. 2020;16(2):194–203.

57 Li C, Shen Y, Huang L, Liu C, Wang J. Senolytic therapy ameliorates renal fibrosis postacute kidney injury by alleviating renal senescence. FASEB J. 2021;35(1):e21229–16.
58 Akhurst RJ. Targeting TGF-β signaling for therapeutic gain. Cold Spring Harb Perspect Biol. 2017;9(10):a022301–30.
59 Shi N, Wang Z, Zhu H, Liu W, Zhao M, Jiang X, et al. Research progress on drugs targeting the TGF-β signaling pathway in fibrotic diseases. Immunol Res. 2022;70(3):276–88.
60 Wang SN, Lapage J, Hirschberg R. Loss of tubular bone morphogenetic protein-7 in diabetic nephropathy. J Am Soc Nephrol. 2001;12(11):2392–9.
61 Tang J, Liu N, Zhuang S. Role of epidermal growth factor receptor in acute and chronic kidney injury. Kidney Int. 2013;83(5):804–10.
62 Li Z, Zhou L, Wang Y, Miao J, Hong X, Hou FF, et al. (Pro)renin receptor is an amplifier of wnt/β-catenin signaling in kidney injury and fibrosis. J Am Soc Nephrol. 2017;28(8):2393–408.
63 Peng X, Xiao Z, Zhang J, Li Y, Dong Y, Du J. IL-17A produced by both γδ T and Th17 cells promotes renal fibrosis via RANTES-mediated leukocyte infiltration after renal obstruction. J Pathol. 2015;235(1):79–89.
64 Peralta CA, Katz R, Bonventre JV, Sabbisetti V, Siscovick D, Sarnak M, et al. Associations of urinary levels of kidney injury molecule 1 (KIM-1) and neutrophil gelatinase-associated lipocalin (NGAL) with kidney function decline in the multi-ethnic study of atherosclerosis (MESA). Am J Kidney Dis. 2012;60(6):904–11.
65 Amdur RL, Feldman HI, Gupta J, Yang W, Kanetsky P, Shlipak M, et al. Inflammation and progression of CKD: the CRIC study. Clin J Am Soc Nephrol. 2016;11(9):1546–56.
66 Eardley KS, Zehnder D, Quinkler M, Lepenies J, Bates RL, Savage CO, et al. The relationship between albuminuria, MCP-1/CCL2, and interstitial macrophages in chronic kidney disease. Kidney Int. 2006;69(7):1189–97.
67 Pawlak K, Kowalewska A, Mysliwiec M, Pawlak D. 3-hydroxyanthranilic acid is independently associated with monocyte chemoattractant protein-1 (CCL2) and macrophage inflammatory protein-1beta (CCL4) in patients with chronic kidney disease. Clin Biochem. 2010;43(13–14):1101–6.
68 Aguiar CF, Naffah-de-Souza C, Castoldi A, Corrêa-Costa M, Braga TT, Naka ÉL, et al. Administration of α-galactosylceramide improves adenine-induced renal injury. Mol Med. 2015;21(1):553–62.
69 Midgley AC, Wei Y, Zhu D, Gao F, Yan H, Khalique A, et al. Multifunctional natural polymer nanoparticles as antifibrotic gene carriers for CKD therapy. J Am Soc Nephrol. 2020;31(10):2292–311.
70 Black LM, Lever JM, Traylor AM, Chen B, Yang Z, Esman SK, et al. Divergent effects of AKI to CKD models on inflammation and fibrosis. Am J Physiol Physiol. 2018;315(4):F1107–18.
71 Brus JE, Quan DL, Wiley KJ, Browning B, Ter Haar H, Lutz R, et al. Diet significantly influences the immunopathology and severity of kidney injury in male C57Bl/6J mice in a model dependent manner. Nutrients. 2021;13(5):1521.
72 Cuadros T, Trilla E, Sarró E, Vilà MR, Vilardell J, de Torres I, et al. HAVCR/KIM-1 activates the IL-6/STAT-3 pathway in clear cell renal cell carcinoma and determines tumor progression and patient outcome. Cancer Res. 2014;74(5):1416–28.
73 Viau A, El Karoui K, Laouari D, Burtin M, Nguyen C, Mori K, et al. Lipocalin 2 is essential for chronic kidney disease progression in mice and humans. J Clin Invest. 2010;120(11):4065–76.
74 Kaleta B. The role of osteopontin in kidney diseases. Inflamm Res. 2019;68(2):93–102.
75 Su H, Lei CT, Zhang C. Interleukin-6 signaling pathway and its role in kidney disease: an update. Front Immunol. 2017;8:405–10.
76 Nakagawa S, Nishihara K, Miyata H, Shinke H, Tomita E, Kajiwara M, et al. Molecular markers of tubulointerstitial fibrosis and tubular cell damage in patients with chronic kidney disease. PLoS One. 2015;10(8):e0136994–14.
77 Lorenzen J, Krämer R, Kliem V, Bode-Boeger SM, Veldink H, Haller H, et al. Circulating levels of osteopontin are closely related to glomerular filtration rate and cardiovascular risk markers in patients with chronic kidney disease. Eur J Clin Invest. 2010;40(4):294–300.
78 Fabian SL, Penchev RR, St-Jacques B, Rao AN, Sipilä P, West KA, et al. Hedgehog-Gli pathway activation during kidney fibrosis. Am J Pathol. 2012;180(4):1441–53.
79 Liu X, Miao J, Wang C, Zhou S, Chen S, Ren Q, et al. Tubule-derived exosomes play a central role in fibroblast activation and kidney fibrosis. Kidney Int. 2020;97(6):1181–95.
80 Kramann R, Fleig SV, Schneider RK, Fabian SL, DiRocco DP, Maarouf O, et al. Pharmacological GLI2 inhibition prevents myofibroblast cell-cycle progression and reduces kidney fibrosis. J Clin Invest. 2015;125(8):2935–51.
81 Di Marco GS, Kentrup D, Reuter S, Mayer AB, Golle L, Tiemann K, et al. Soluble Flt-1 links microvascular disease with heart failure in CKD. Basic Res Cardiol. 2015;110(3):30.
82 Neder TH, Schrankl J, Fuchs MAA, Broeker KAE, Wagner C. Endothelin receptors in renal interstitial cells do not contribute to the development of fibrosis during experimental kidney disease. Pflugers Arch. 2021;473(10):1667–83.
83 Feng Y, Ren J, Gui Y, Wei W, Shu B, Lu Q, et al. Wnt/β-Catenin–Promoted macrophage alternative activation contributes to kidney fibrosis. J Am Soc Nephrol. 2018;29(1):182–93.
84 Chaabane W, Praddaude F, Buleon M, Jaafar A, Vallet M, Rischmann P, et al. Renal functional decline and glomerulotubular injury are arrested but not restored by release of unilateral ureteral obstruction (UUO). Am J Physiol Ren Physiol. 2013;304(4):432–9.
85 Nangaku M, Kitching AR, Boor P, Fornoni A, Floege J, Coates PT, et al. International Society of Nephrology first consensus guidance for preclinical animal studies in translational nephrology. Kidney Int. 2023;104(1):36–45.